Cell
PRESS

A Full-Length Group 1 Bacterial Sigma Factor Adopts a Compact Structure Incompatible with DNA Binding

Edmund C. Schwartz,[1] Alexander Shekhtman,[2,4] Kaushik Dutta,[2] Matthew R. Pratt,[1] David Cowburn,[2] Seth Darst,[3] and Tom W. Muir[1,*]

[1]Laboratory of Synthetic Protein Chemistry, The Rockefeller University, 1230 York Avenue, New York, NY 10021, USA
[2]New York Structural Biology Center, New York, NY 10027, USA
[3]Department of Molecular Biophysics, The Rockefeller University, 1230 York Avenue, New York, NY 10021, USA
[4]Present address: Department of Chemistry, State University of New York at Albany, 1400 Washington Avenue, Rm LSB1148, Albanym NY 12222, USA
*Correspondence: muirt@rockefeller.edu
DOI 10.1016/j.chembiol.2008.09.008

SUMMARY

The σ factors are the key regulators of bacterial transcription initiation. Through direct read-out of promoter DNA sequence, they recruit the core RNA polymerase to sites of initiation, thereby dictating the RNA polymerase promoter-specificity. The group 1 σ factors, which direct the vast majority of transcription initiation during log phase growth and are essential for viability, are autoregulated by an N-terminal sequence known as $\sigma_{1.1}$. We report the solution structure of *Thermotoga maritima* σ^A $\sigma_{1.1}$. We additionally demonstrate by using chemical crosslinking strategies that $\sigma_{1.1}$ is in close proximity to the promoter recognition domains of σ^A. We therefore propose that $\sigma_{1.1}$ autoinhibits promoter DNA binding of free σ^A by stabilizing a compact organization of the σ factor domains that is unable to bind DNA.

INTRODUCTION

The catalytically competent core bacterial RNA polymerase (RNAP, subunit composition $\alpha_2\beta\beta'\omega$) is unable to initiate promoter-specific transcription (Borukhov and Nudler, 2003; Browning and Busby, 2004; Darst, 2001; Ebright, 2000; Gross et al., 1998; Murakami and Darst, 2003). Transcription initiation requires an additional subunit, the σ factor, to form the RNAP holoenzyme (Burgess et al., 1969; Travers and Burgess, 1969). The σ factor confers upon the RNAP holoenzyme the ability to recognize and bind promoter DNA, and also plays a key role in dsDNA melting to form the transcription bubble, allowing transcription initiation.
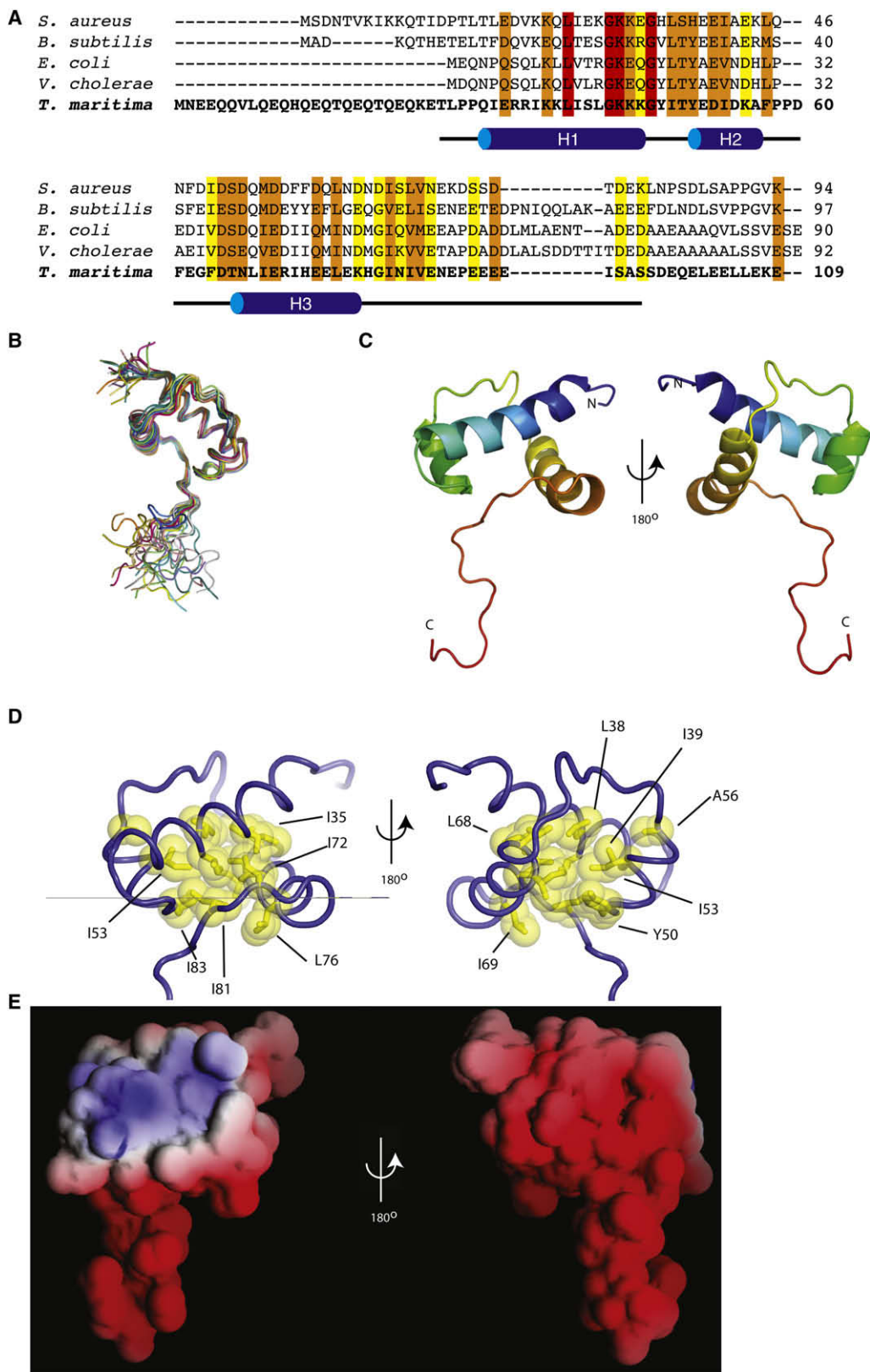
Bacterial species have anywhere from a single σ factor to more than 60 that, together with various transcription factors, regulate different transcriptional responses and programs (Borukhov and Nudler, 2003; Browning and Busby, 2004; Gruber and Gross, 2003). The σ factors fall into two broad classes, the σ^{70} family and the σ^{54} family (Gruber and Gross, 2003). Only the σ^{70} family members are present in all bacterial species. The σ^{70} family is further subdivided into four groups. The group

1, or primary, σ factors are responsible for the bulk of transcription during log phase growth and are essential for viability, whereas group 2-4 σ factors, or alternate, σ factors fulfill more specialized functions such as stress responses (Gruber and Gross, 2003).

The σ factors need to be regulated in order to prevent DNA binding at inappropriate times. Specialized σ factors are often regulated through binding to anti-σ factors that prevent them from interacting with core RNAP and contacting DNA (reviewed in Campbell and Darst, 2005; Campbell et al., 2008). The group 1 σ factors do not bind promoter DNA before the formation of the RNAP holoenzyme, due in large part to an N-terminal extension that is unique to group 1 σ factors called $\sigma_{1.1}$ (Camarero et al., 2002; Dombroski et al., 1992, 1993).

The group 1 σ factors contain four conserved domains, known as $\sigma_{1.1}$, σ_2, σ_3, and σ_4, connected by flexible linkers. A wealth of structural and biochemical information is available on σ_2, σ_3, and σ_4 (Campbell et al., 2002a, 2002b, 2003; Lane and Darst, 2006; Malhotra et al., 1996; Murakami et al., 2002a, 2002b; Sorenson et al., 2004; Vassylyev et al., 2002). σ_2 recognizes the promoter -10 element and plays an essential role in the melting of the double-stranded DNA to form the transcription bubble (Gross et al., 1998). σ_3 recognizes the extended -10 element (Barne et al., 1997). σ_4 recognizes the promoter -35 element (Gardella et al., 1989; Siegele et al., 1989). These three domains also form extensive contacts with the core RNAP (Murakami et al., 2002a, 2002b; Vassylyev et al., 2002). There is no structural information available on $\sigma_{1.1}$. However, biochemical information shows that it plays a role in the transition from a closed to an open promoter complex (Vuthoori et al., 2001; Wilson and Dombroski, 1997) and is responsible for preventing DNA binding prior to formation of the holoenzyme (Camarero et al., 2002; Dombroski et al., 1992, 1993).

The mechanism by which $\sigma_{1.1}$ prevents DNA binding by the group 1 σ factors is unknown. σ constructs lacking $\sigma_{1.1}$ are able to bind promoter DNA whereas full-length group 1 σ factors exhibit only very weak DNA binding (Camarero et al., 2002; Dombroski et al., 1992, 1993). Additionally, $\sigma_{1.1}$ can interfere with DNA binding by σ_4 in *trans* (Dombroski et al., 1993). This led to the proposal that $\sigma_{1.1}$ binds to σ_4 to prevent -35 element binding. However, an NMR-based study was unable to detect a direct interaction between $\sigma_{1.1}$ and the C-terminal portion of σ_4, $\sigma_{4.2}$,

A
```
S. aureus      ------------MSDNTVKIKKQTIDPTLTLEDVKKQLIEKGKKEGHLSHEEIAEKLQ--  46
B. subtilis    ------------MAD------KQTHETELTFDQVKEQLTESGKKRGVLTYEEIAERMS--  40
E. coli        -------------------------MEQNPQSQLKLLVTRGKEQGYLTYAEVNDHLP--  32
V. cholerae    -------------------------MDQNPQSQLKQLVLRGKEQGYLTYAEVNDHLP--  32
T. maritima    MNEEQQVLQEQHQEQTQEQTQEQKETLPPQIERRIKKLISLGKKKGYITYEDIDKAFPPD  60
```

```
S. aureus      NFDIDSDQMDDFFDQLNDNDISLVNEKDSSD----------TDEKLNPSDLSAPPGVK--  94
B. subtilis    SFEIESDQMDEYYEFLGEQGVELISENEETEDPNIQQLAK-AEEEFDLNDLSVPPGVK--  97
E. coli        EDIVDSDQIEDIIQMINDMGIQVMEEAPDADDLMLAENT--ADEDAAEAAAQVLSSVESE  90
V. cholerae    AEIVDSEQVEDIIQMINDMGIKVVETAPDADDLALSDDTTITDEDAAEAAAAALSSVESE  92
T. maritima    FEGFDTNLIERIHEELEKHGINIVENEPEEEE---------ISASSDEQELEELLEKE--  109
```

B
C

D

E

which harbors the −35 element DNA binding determinants (Camarero et al., 2002). In addition, no interaction between $\sigma_{1.1}$ and σ_4 could be detected using a bacterial two-hybrid screen (Hinton et al., 2006). Thus, it is also possible that $\sigma_{1.1}$ prevents DNA binding through an allosteric mechanism, or that $\sigma_{1.1}$ does not interact with other domains of the σ factor and DNA binding is prevented simply by electrostatic repulsion between the highly negatively charged $\sigma_{1.1}$ and negatively charged DNA.

Here we report the solution structure of $\sigma_{1.1}$ of *T. maritima* σ^A. We also demonstrate, through intramolecular crosslinking, that $\sigma_{1.1}$ is in close proximity to the DNA binding domains σ_2 and σ_4 in the autoinhibited state. We propose that $\sigma_{1.1}$ interdomain contacts stabilize a compacted σ factor structure that is sterically incompatible with DNA binding.

RESULTS

$\sigma_{1.1}$ Adopts a Novel Helical Fold

All of our studies were carried out using derivatives of σ^A from *T. maritima (Tm)*. This σ factor has a high degree of sequence similarity to σ^{70} from *E. coli*, including throughout $\sigma_{1.1}$ (Figure 1A), but is thermostable and lacks a 240 residue non-conserved insertion between $\sigma_{1.2}$ and σ_2 present in *Ec* σ^{70} so is considerably smaller (47 kDa versus 70 kDa), making it better suited for biochemical and structural studies (Camarero et al., 2002). Based on sequence alignments, $\sigma_{1.1}$ of *Tm* σ^A extends approximately from residue 25 to residue 120 (Figure 1A). Preliminary NMR experiments revealed that the non-conserved N-terminus of σ^A (residues ~1-30) and the C terminus of $\sigma_{1.1}$ (~95-120) were unstructured (data not shown). Thus, the construct we ultimately used for structural determination contained residues 29-95. Uniformly ^{15}N and ^{13}C labeled σ^A(29-95) was used to obtain the main- and side-chain assignments of the ^1H, ^{15}N, and ^{13}C resonances using the standard set of double- and triple-resonance 2D and 3D experiments (Cavanagh et al., 1996). An initial assessment of the $\sigma_{1.1}$ secondary structure was made using the deviations of assigned chemical shifts from random coil values (Wishart and Sykes, 1994). This analysis suggested that the domain was composed entirely of α-helical secondary structure elements.

The solution structure of $\sigma_{1.1}$ (pdb accession 2K6X) was solved using restraints generated from a series of multi-dimensional NMR experiments. Structure calculations were performed using a total of 877 unambiguous distance restraints (245 intraresidue, 314 sequential, 185 short range, 40 medium range and 93 long range). In addition, 107 dihedral (ϕ and ψ) angle restraints and 44 hydrogen bond restraints were used in the structure calculations. Structural statistics and analysis are given in Table 1 and the 20 lowest energy structures are superimposed

Table 1. NMR Restraints and Structural Statistics for the Best 20 Structures

Restraints and Statistics	
Total number of restraints	1028
NOE restraints	877
Intraresidue	245
Sequential	314
Short-range	185
Medium-range	40
Long-range	93
Dihedral angle restraints	107
Hydrogen bond restraints[a]	44
Structure statistics[b]	
NOE violations > 0.5 Å	0
Dihedral violations > 5°	0
Total energy (kcal/mol)	−2498.83 ± 48.09
NOE constraints energy (kcal/mol)	76.07 ± 10.59
RMSD from Average Structure[c,d] **All residues (236–298)**	
Backbone (N, Cα, C) (Å)	0.56 ± 0.11 (2.07 ± 0.54)
Heavy atoms (Å)	1.25 ± 0.14 (2.45 ± 0.46)
Ramachandran Statistics[e]	
Most favored region (%)	96.4 (85.5)
Additionally allowed (%)	3.6 (12.7)
Generously allowed (%)	0.0 (1.0)
Disallowed (%)	0.0 (0.8)

[a] Hydrogen bond restraints were H^N-O distance of 1.8–2.3 Å and an N-O distance of 2.8–3.3 Å.
[b] Structural characteristics for the final ensemble of 20 water-refined structures.
[c] RMSD of the mean structure from individual structures in the ensemble.
[d] RMSD for residues 29–86. The numbers in the parenthesis indicate the RMSD for residues 29–95.
[e] Ramachandran plot data shown for residues 29–86. The numbers in parentheses indicate the statistics for residues 29–95.

in Figure 1B. For the structured region, (residues 29-86) the average pairwise root-mean-square deviation (RMSD) is 0.56 ± 0.11 Å for backbone residues and 1.25 ± 0.14 Å for all heavy atoms. Most of the residues are in the most favored (85.5%) or allowed (12.7%) conformations. Proline 58, which is largely but not universally conserved between σ factors, is in the *cis* conformation based on H_α-H_δ/$H_{d'}$ NOE data.

$\sigma_{1.1}$ possesses a novel fold comprising three α helices connected by two loops (Figure 1C). Helix 1 (H1) is the longest helix and contains residues Q30-K45. H1 is connected by a four-residue loop to the smallest helix (H2) comprising residues Y50-A56.

Figure 1. Structure of $\sigma_{1.1}$

(A) An alignment of $\sigma_{1.1}$ from five different bacterial species generated using the ClustalW program. Highlighted in red are identical residues, in orange are conserved residues and in yellow are semiconserved residues. The black line below the alignment represents the construct used for structural determination, with secondary structural elements (H1-H3) indicated.

(B) A superimposition of the backbone of the 20 lowest energy structures of $\sigma_{1.1}$ obtained from calculations using NMR-derived restraints. Each structure is individually colored. The N-termini are in the upper left and the C-termini are in the bottom half of the figure.

(C) Cartoon representation of the secondary structure elements of $\sigma_{1.1}$. The structure is rainbow spectrum colored from N-terminus (blue) to C terminus (red).

(D) Cartoon representation of $\sigma_{1.1}$. Residues that form the hydrophobic core are shown in yellow. Images generated using MacPYMOL (Delano Scientific).

(E) Electrostatic surface of $\sigma_{1.1}$. Red is negative, blue is positive, and white is neutral. Image generated using GRASP (Nicholls et al., 1991).
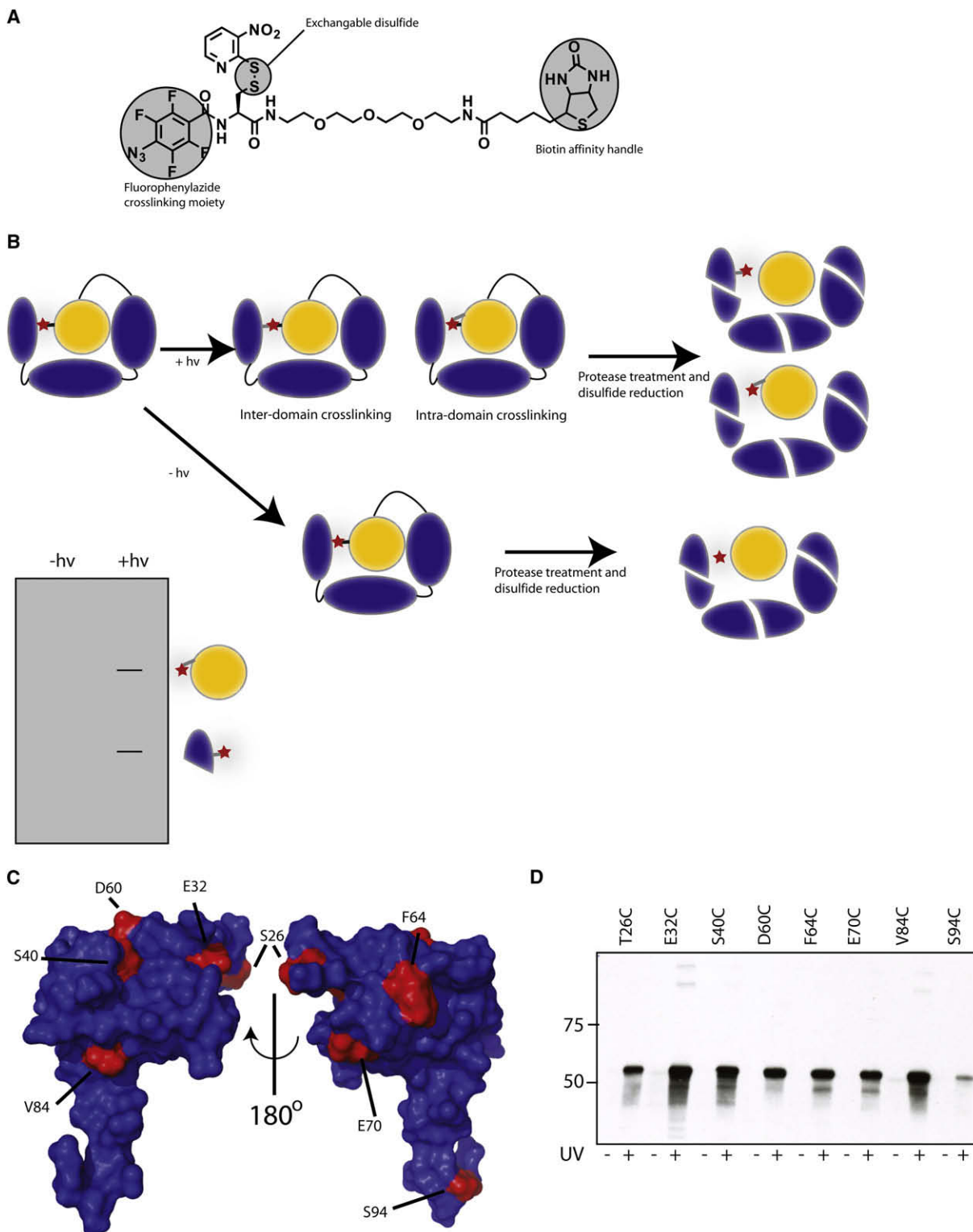
Figure 2. Crosslinking to detect intramolecular interactions

(A) Chemical structure of the photo-crosslinker used in this study. A synthetic scheme is provided in supplemental material.

(B) The crosslinker (red star) is attached by disulfide exchange to a surface cysteine in the σ factor. Following photo-crosslinking and digestion, the disulfide is reduced, transferring the tag to regions in close proximity to $\sigma_{1.1}$. The transferred tag is detected by electrophoretic methods.

(C) $\sigma_{1.1}$ residues mutated for crosslinking studies. The surface of $\sigma_{1.1}$ is rendered in blue with residues that were mutated to cysteine for attachment of the crosslinker highlighted in red. Images were generated using MacPYMOL (Delano Scientific).

H2 is connected via an eight-residue loop to the final helix (H3), which stretches from residues T66-K78. H2 and H3 are roughly anti-parallel to one another and pack perpendicularly against H1. $\sigma_{1.1}$ contains a compact hydrophobic core formed by highly conserved residues from all three helices and part of the C-terminal tail (Figure 1D). Indeed, the side-chains of I81 and I83, from the tail, project directly into the hydrophobic core where they pack against residues from all three helices. These interactions help to hold residues 79-83 of the tail in an extended conformation that runs roughly parallel with H1. The apparent structural role of I81 is particularly interesting since the corresponding residue in *E. coli* σ^{70} (I53) has been shown to be required for its function (Bowers and Dombroski, 1999). As expected from the amino acid composition, $\sigma_{1.1}$ has a mostly negative electrostatic surface potential (Figure 1E). An intriguing exception to this is a positively charged patch centered on H1. The functional relevance of this will be discussed in later sections.

$\sigma_{1.1}$ Makes Interdomain Contacts

We next turned to the question of whether region 1.1 makes contacts with other domains in the σ factor. Our initial approach to this problem was to use NMR spectroscopy employing segmental isotopic labeled σ^{A} constructs prepared using expressed protein ligation (Muralidharan and Muir, 2006; Ottesen et al., 2003). Although the NMR spectra obtained using these constructs were consistent with there being inter-domain interactions involving σ-1.1, the data were insufficient to determine the details of these interactions (see Figures S1 and S2 available online). Despite considerable efforts to overcome these technical issues, we concluded that an alternative methodology was needed to unambiguously characterize the putative inter-domain interactions in the sigma factor.

We decided that a site-directed crosslinking strategy might be a more productive approach to this problem. Our approach exploits the fact the *Tm* σ^{A} contains no native cysteines, a feature which should allow selective attachment of a chemical crosslinker to a mutant cysteine introduced into $\sigma_{1.1}$. With this in mind, we synthesized a novel crosslinker containing a fluorophenylazide photo-reactive warhead, a 3-nitro-2-pyridinesulfenyl group for attachment to the protein through disulfide exchange, and a biotin handle for downstream detection (Figure 2A, Figure S3). Once attached to the cysteine sulfhydryl, the reactive azide within the crosslinker is separated from the side-chain by a distance of ~14 Å. The crosslinking strategy we devised is based on transfer of the biotin tag from $\sigma_{1.1}$ to another domain upon irradiation and reduction (Figure 2B). In principle, the tagged domain could then be identified by electrophoretic or mass spectrometry resolution of the fragments produced by proteolytic or chemical cleavage methods.

Using the structure of $\sigma_{1.1}$ as a guide, we selected ten residues to mutate to cysteine for crosslinker attachment (Figure 2C). These were designed to give broad coverage of the surface of $\sigma_{1.1}$. Of the ten point mutations made, eight could be expressed and purified (Figure S4 and Table S1). The E51C and E77C mutants did not express. The mutant proteins were then labeled

with crosslinker using a disulfide exchange process (Figure 2D). In all cases, the crosslinker could be removed by reduction with DTT before but not after ultraviolet irradiation at 325 nm, indicating that crosslinking to the protein had occurred. Moreover, we observed no evidence of the formation of crosslinked σ^{A} dimers or higher oligomers (Figure S5), indicating that under the conditions of all our experiments, crosslinking is intramolecular. The presence of the label did not interfere with DNA binding autoinhibition by $\sigma_{1.1}$ in any of the mutants (Figure S6A). Furthermore, labeled σ factors behaved as wild-type in abortive transcription initiation assays (Figure S6B).

Having established that crosslinks from $\sigma_{1.1}$ could be formed, we next set about determining what portions of the σ factor were being contacted by $\sigma_{1.1}$. Numerous attempts were made to directly identify crosslinked regions by mass spectrometry analysis of tryptic fragments, but in no case could the unambiguous identification of a crosslinked peptide be made. We thus turned to gel-based methods to map the sites of crosslinking. Analysis of the σ^{A} sequence suggested that cyanogen bromide (CNBr) digestion of the protein would be informative. The expected CNBr digestion pattern is shown in Figure 3A. The majority of crosslinking is predicted to occur locally, to nearby portions of $\sigma_{1.1}$. Fortunately, $\sigma_{1.1}$ is entirely contained within a single CNBr fragment that is more than twice as large as the next largest fragment. Thus, $\sigma_{1.1}$ should be easily resolved from other CNBr fragments by SDS-PAGE, in principle, allowing one to distinguish between local and interdomain crosslinking.

In order to map protein crosslinking site(s), the irradiated samples were digested with CNBr followed by reduction to transfer the biotin tag. In all cases, western blotting revealed the presence of biotin-probe on fragments that contain $\sigma_{1.1}$ (Figure 3B). Several of the CNBr digestion fragments of σ^{A}, including $\sigma_{1.1}$, migrate slower than predicted based on molecular weight (a detailed description of the procedure used to identify the CNBr digestion products is provided in the Supplemental Data). Labeling of $\sigma_{1.1}$ is consistent with local crosslinking, which was expected. The presence of biotin in bands that were smaller than the $\sigma_{1.1}$ was interpreted to indicate interdomain crosslinks. By this criterion, the E32C and S40C attachment sites did not display strong crosslinking to fragments from any other region. By contrast, the other mutants all showed crosslinking to fragments that were smaller than $\sigma_{1.1}$, and must therefore come from domains 2-4. Crosslinking from the D60C and F64C attachment sites led to labeling of a ~6 kDa band that was unambiguously assigned to $\sigma_{4.2}$ (R[342-399]G and R[342-394]M) by mass spectrometry. Additionally, crosslinking from the T26C, D60C, F64C, E70C, and V84C attachment sites led to robust labeling of a fragment with an apparent mobility between 10 and 15 kDa. This mobility is consistent with fragments from either σ_2 or σ_3. However, it is also possible that partial digestion products containing σ_4 could account for some of the bands observed between 10 and 15 kDa.

To help resolve this ambiguity, we turned to BNPS-skatole (2-[2′-nitrophenylsulfenyl]-3-methyl-3-bromoinolenine) digestion, which cleaves following tryptophan residues. There are three tryptophan residues in σ^{A}: W201, W213, and W214. Thus,

---

(D) Crosslinking can be induced by ultraviolet irradiation. Indicated σ^{A} mutants were labeled with crosslinker by disulfide exchange. Samples that had either been irradiated or had not been irradiated at 325 nm light were then reduced with DTT. Samples were then resolved by SDS-PAGE and analyzed by western blot (streptavidin-HRP).
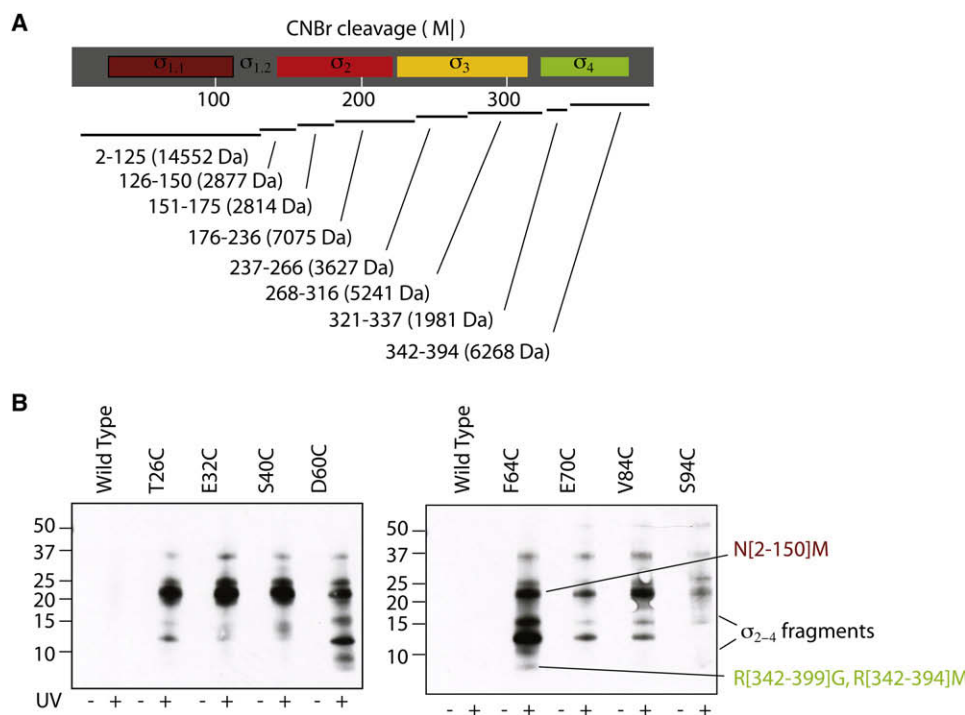
Figure 3. Interdomain crosslinking from $\sigma_{1.1}$

(A) Predicted CNBr digestion of *Tm* σ^A. The domain structure of σ^A (top) is shown with the predicted CNBr digestion fragments below. Residue numbers of cleavage products are shown with molecular weights in parentheses.

(B) Photo-crosslinking from $\sigma_{1.1}$ analyzed by label transfer and CNBr digestion. Crosslinker was attached at the indicated residues within $\sigma_{1.1}$ through a disulfide. Wild-type σ^A, which lacks a native cysteine, was included as a control. Irradiated (UV+) and nonirradiated (UV-) samples were digested with CNBr, separated by reducing SDS-PAGE (10%–20% acrylamide, Tris-tricine buffer system) and probed for biotin by western blotting (HRP-streptavidin). Only the irradiated cysteine mutants retained the biotin. The identity of the labeled bands is shown at right. Bands that have been identified by mass spectrometry are labeled with residue numbers. A full account of the assignment protocol is given in Supplemental Methods.

BNPS-skatole digestion effectively cuts σ^A in half (Figure 4A). Crosslinked protein samples were digested with BNPS-skatole, separated by reducing SDS-PAGE and blotted with streptavidin-HRP (Figure 4B). As expected, when the crosslinker was attached to residues 32 or 40, very little labeling was seen on the band representing the C-terminal half of the protein (202/215-399). In contrast, label-transfer to the C-terminal fragment clearly occurred when the crosslinker was attached to the other six sites, indicating interdomain crosslinking. In all cases, crosslinking was observed to the N-terminal fragment of the protein, comprising residues 1-201/214 (Figure 4B). This is consistent with the formation of local crosslinks to $\sigma_{1.1}$, but could also represent crosslinking to σ_2.

To further map the interactions, a subset of the crosslinked samples was subjected to a two-stage digestion procedure. We chose E32C, F64C, and E70C as representatives of what appears to be three distinct crosslinking patterns (Figure 3B). Following BNPS-skatole digestion, the bands corresponding to the N- and C- fragments were cut out of the Coomassie-stained gel, extracted, and digested with CNBr before being analyzed by blotting with HRP-streptavidin. For the F64C and E70C crosslinker attachment sites, CNBr digestion of the C-terminal BNPS-skatole fragment led to the generation of smaller biotin-containing fragments (Figure 4C). From this we can conclude that $\sigma_{1.1}$ is situated close to σ_3 and/or σ_4 in the autoinhibited state.

In the case of F64C, the labeling pattern includes the $\sigma_{4.2}$ fragment previously seen in the CNBr digestion of the intact protein. No biotin-labeled fragments were detected in the extracted and digested C-fragment from the E32C mutant, which is consistent with the finding that no interdomain crosslinking occurs from this attachment site. CNBr digestion of the BNPS-skatole N-fragment was more revealing. Although the E32C attachment site showed no crosslinking to smaller digestion fragments, the F64C and E70C sites both displayed faint, but reproducible, biotin-labeled fragments with greater gel mobility than $\sigma_{1.1}$ (Figure 4D). These can only represent digestion fragments containing σ_2, suggesting that $\sigma_{1.1}$ and σ_2 are close in space.

$\sigma_{1.1}$ and σ_4 Are Close in Space

To confirm that $\sigma_{1.1}$ is proximal to σ_4, we performed crosslinking experiments in the reverse direction, i.e., from σ_4 back to $\sigma_{1.1}$. Using the structure of the highly homologous σ_4 from *Thermus aquaticus* as a guide (Campbell et al., 2002b), we designed two surface exposed sites for crosslinker attachment, E365 and V372, both of which are located in $\sigma_{4.2}$. The corresponding cysteine mutants (E365C and V372C) were generated (Figure S4) and crosslinking/label-transfer experiments performed as with the $\sigma_{1.1}$ mutants. As expected, local crosslinking to σ_4 was observed in both cases (Figure 5A). More importantly, we also observed substantial crosslinking to $\sigma_{1.1}$ from the V372C

attachment site, based on the appearance of a biotin-labeled $\sigma_{1.1}$ fragment in the CNBr digest. There was no evidence of crosslinks from the E365C site back to $\sigma_{1.1}$. This difference in behavior may reflect the fact that E365C, but not V372C, is highly conserved in group 1 σ factors, and so the structure and/or function of σ_4 may be more sensitive to perturbations at this site. The key result, however, is the observation of crosslinks to $\sigma_{1.1}$ from position 372, which serves to confirm that $\sigma_{1.1}$ is situated near σ_4 in the autoinhibited state.

$\sigma_{1.1}$, σ_2, and σ_4 Are Situated Close in Space

Because the crosslinks between $\sigma_{1.1}$ and σ_2 were identified following double digestion and were only faintly detected, we felt it was particularly important to confirm these by showing crosslinking in the reverse direction. Accordingly, we generated four cysteine mutants of σ_2 for crosslinker attachment (Figure S4). These were designed to give broad surface coverage based on the structure of the homologous σ_2 from *T. aquaticus* (Campbell et al., 2002b). These samples were crosslinked and analyzed as with the $\sigma_{1.1}$ and σ_4 mutants (Figure 5B). For the D183C, K198C, and D225C attachment sites, the predominant labeled band migrated between 10 and 15 kDa. We reasoned that this fragment likely results from local crosslinking and as such corresponds to the CNBr fragment of σ_2 containing the crosslinker attachment sites, i.e., G[176-236]M. Consistent with this interpretation, this band was completely absent in the digest from the R165C attachment site from which local crosslinking affords a CNBr fragment of only 2.8 kDa, which would not be seen in this figure. More importantly, we observed crosslinking from σ_2 back to $\sigma_{1.1}$ for all four crosslinker attachment sites (Figure 5B). This is clearly illustrated for the R165C attachment site where the principle labeled band in the CNBr digest migrates at the position that corresponds to $\sigma_{1.1}$. Additionally, we observed crosslinking from σ_2 to $\sigma_{4.2}$. Such crosslinks could not be unambiguously assigned when performing crosslinking from the σ_4 mutants, due to the possibility of detecting partial digestion products containing σ_4. However, because the $\sigma_{4.2}$ bands display unique gel mobility, they could be easily identified in this experiment.

DISCUSSION

The DNA binding functions of bacterial σ factors are regulated through a variety of mechanisms (Gruber and Gross, 2003). The group 1 σ factors, which perform the bulk of transcription during exponential growth, are converted from an autoinhibited state, which cannot interact with promoter DNA, to an active form that recognizes promoter DNA upon binding to core RNAP. Biochemical and genetic studies have established that the N-terminal domain of group 1 σ factors, $\sigma_{1.1}$, is required for autoinhibition (Dombroski et al., 1992, 1993). The mechanistic basis for this $\sigma_{1.1}$ function has remained unclear. Biochemical studies indicate that $\sigma_{1.1}$ can inhibit the DNA binding properties of σ_4 in *trans*, suggesting a direct physical interaction between the domains (Dombroski et al., 1993; Dombroski et al., 1992). However, NMR studies of segmental labeled versions of *Tm* σ^A do not support a direct interaction between $\sigma_{1.1}$ and at least the C-terminal half of σ_4 (Camarero et al., 2002). In the present study, we have shown that, in the autoinhibited state, $\sigma_{1.1}$ of *Tm* σ^A is in close proximity to both DNA binding domains of

the protein, namely σ_2 and σ_4. Critical to these studies was the determination of the solution structure of $\sigma_{1.1}$, because this allowed us to rationally design point mutants of the protein for use in a site-directed chemical crosslinking strategy employing a novel trifunctional chemical crosslinking reagent.

Although there is no structure available of an intact, isolated group 1 σ factor, the crystal structure of a full-length alternative sigma factor from *Aquifex aeolicus*, σ^{28}, has been solved in complex with its anti-sigma factor FlgM (Sorenson et al., 2004). σ^{28} has a highly compacted structure in this complex, with extensive interfaces between conserved σ_{2-4}. Biochemical studies suggest that σ^{28} maintains this compacted structure even in the absence of FlgM (Sorenson and Darst, 2006). This led to the proposal that autoinhibition of DNA binding in σ^{28} results from a combination of suboptimal interdomain distances and steric occlusion of the promoter binding determinants. An obvious question then is whether similar interdomain interactions exist in autoinhibited group 1 σ factors. The high level of sequence homology between σ_2 and σ_4, and to a lesser extent σ_3, argues in favor of a similar compacted structure. However, because alternative σ factors like σ^{28} lack $\sigma_{1.1}$, it is quite possible that a different arrangement of the domains is present in autoinhibited group 1 σ factors. We observed direct crosslinks between σ_2 and σ_4 in free σ^A (Figure 5), which is consistent with a σ^{28}-like structure. However, given the low resolution of crosslinking experiments, it is unclear whether this reflects a direct physical interaction between these domains or close apposition without actual contact. In the structure of σ^{28}, the C-terminal portion of σ_3 (which is highly acidic in both primary and alternative σ factors) forms a bent helix that sits between σ_2 and σ_4 and packs against the basic −35 element binding region of σ_4. Therefore, we would expect to see crosslinks to σ_3 if σ^A assumes a similar structure as σ^{28}. Unfortunately, it was not possible to unambiguously assign crosslinked bands to σ_3 fragments using the chemical cleavage methods we employed. Thus, although we cannot rule out such crosslinks, the question of whether part of σ_3 inserts between σ_2 and σ_4 in σ^A remains unclear.

Our crosslinking data indicate that $\sigma_{1.1}$ packs close to σ_2 and σ_4 in the autoinhibited state of σ^A, and that surface electrostatics play a role in this compaction. As expected, based on the highly acidic sequence of $\sigma_{1.1}$ (calculated pI = 4.4), the majority of the protein surface is negatively charged. However, there also exists a small positively charged patch centered on H1 (Figure 1E). Of the eight sites in $\sigma_{1.1}$ chosen for crosslinker attachment, all but two exhibited interdomain crosslinking (Figure 3). What is remarkable is how this apportioning of activity correlates with surface electrostatics; all the sites from which interdomain crosslinking was observed map to the negative surface, whereas both of the sites from which no interdomain crosslinking was observed map to the positive patch (Figure 6A). σ_2 and σ_4 are both positively charged DNA binding domains (calculated pIs for σ_2 and σ_4 are 10.5 and 10, respectively). It is therefore likely that electrostatic forces play an important role in stabilizing the close proximity of $\sigma_{1.1}$, σ_2, and σ_4 revealed by our crosslinking data. Consistent with this idea, the autoinhibitory effect of $\sigma_{1.1}$ is known to be highly sensitive to changes in ionic strength (Camarero et al., 2002).

Our crosslinking data present a picture of the free group 1 σ factor that is very different from the structure in the RNAP
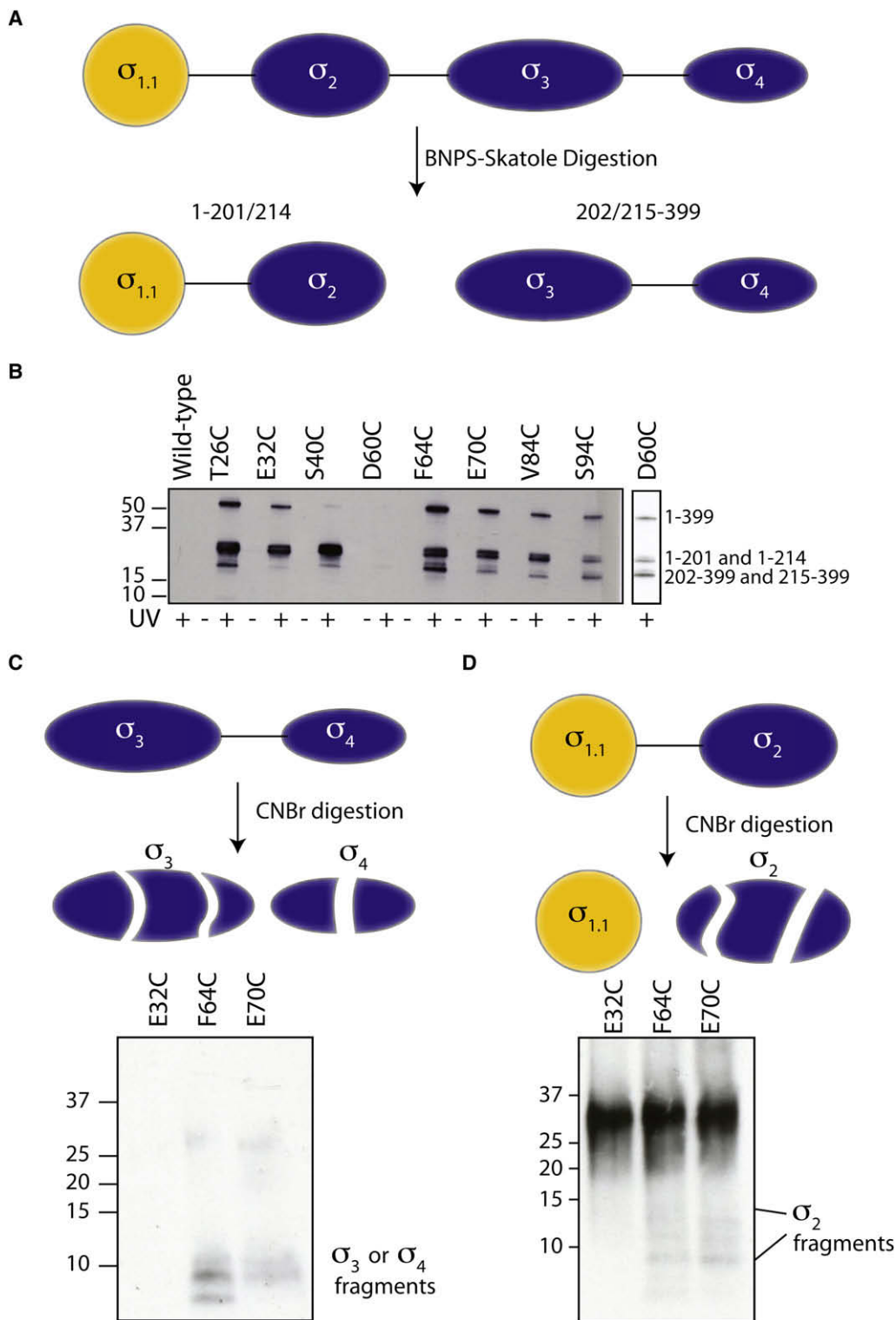
Figure 4. BNPS-Skatole and two-stage digestion of crosslinked products

(A) BNPS-Skatole cleaves after Trp residues and, as a consequence, conveniently cuts σ^A between σ_2 and σ_3.

(B) Photo-crosslinking from $\sigma_{1.1}$ analyzed by label transfer and BNPS digestion. Crosslinker was attached at the indicated residues within $\sigma_{1.1}$ through a disulfide. Wild-type σ^A, which lacks a native cysteine, was included as a control. Irradiated (UV+) and nonirradiated (UV-) samples were digested with BNPS, separated by reducing SDS-PAGE (4–12% acrylamide) and probed for biotin by western blotting (HRP-streptavidin). The D60C sample did not label well, so a longer exposure is shown to the right. The identity of the labeled bands (shown at right) was determined by in-gel trypsinolysis followed by mass spectrometry (data not shown).

holoenzyme. In the latter context, the σ factor adopts an extended conformation, with each domain widely separated in space (Murakami et al., 2002a; Vassylyev et al., 2002). For instance, in the crystal structure of the *Thermus thermophilus* holoenzyme, the centers of σ_2 and σ_4 are separated by $\sim$65 Å (versus $\sim$25 Å in the structure of σ^{28}), and $\sigma_{1.1}$, which is not resolved in the structure, is believed to be separated from the rest of the holoenzyme by a flexible linker (Vassylyev et al., 2002). By contrast, our crosslinking data indicate that the domains in the free σ factor are in close proximity; $\sigma_{1.1}$, σ_2, and σ_4 all crosslink to one another. We again stress that the presence of these crosslinks does not prove that all of the domains are physically interacting, particularly because the attachment chemistry results in a $\sim$14 Å linker between the cysteine and the reactive azide group. Nonetheless, the crosslinking data are clearly incompatible with the open conformation of σ^A found in the holoenzyme structures. Rather, our data suggest that the free factor assumes a much more compacted state relative to the conformation in the holoenzyme. This idea is also supported by LRET and FRET studies on *E. coli* σ^{70}, which indicate that the interdomain distances are considerably smaller in free σ than in the RNAP holoenzyme (Callaci et al., 1999; Mekler et al., 2002).

The crosslinking data presented herein, together with the aforementioned biochemical and biophysical studies, point to an autoinhibition mechanism involving a significant compaction of the free σ factor relative to its more open conformation in the holoenzyme. Because interdomain crosslinks were only observed from the negative surface of $\sigma_{1.1}$, we propose that electrostatic interactions between this surface and the positively charged surfaces of σ_2 and σ_4 underlie this compaction (Figure 6B). The autoregulatory role of $\sigma_{1.1}$ is therefore fulfilled by locking the DNA binding domains in a conformation that is incompatible with promoter binding. We cannot, using the approaches we have employed, determine the strength of the interactions between $\sigma_{1.1}$ and the DNA binding domains of the σ factor. We predict, however, that they are fairly weak, and likely transient, for a number of reasons. First, mechanistically, the interdomain interactions need to be broken in order to form the DNA binding competent RNAP holoenzyme. If the interactions between the sigma domains are of high affinity, it would be energetically expensive to form productive holoenzyme complexes due to effective molarity (Kobe and Kemp, 1999). Second, although σ constructs containing σ_4 could be inhibited by the addition of $\sigma_{1.1}$ in *trans*, achieving a 50% reduction in DNA binding required a 15- to 20-fold excess of $\sigma_{1.1}$ over σ_4, suggesting that binding between the two domains is weak (Dombroski et al., 1993). Additionally, σ_2 binding by $\sigma_{1.1}$ could not be detected in this *trans* inhibition assay, once again implying weak binding. Finally, the NMR spectra of $\sigma_{4.2}$ are not significantly perturbed by $\sigma_{1.1}$ (Camarero et al., 2002), despite the fact that our crosslinking data show that $\sigma_{1.1}$ and $\sigma_{4.2}$ must be in close proximity. This points to an interaction that is both weak and somewhat fluid, which could be difficult to detect when using NMR-based approaches. This highlights the sensitivity of the crosslinking approach because it can capture relatively weak and transient interactions.

SIGNIFICANCE

In this work, we have reported the first high-resolution structure of a $\sigma_{1.1}$ domain. Although there is a wealth of structural data on bacterial sigma factors and fragments thereof, to date there had been no structure available on $\sigma_{1.1}$. We have addressed a longstanding mechanistic issue in prokaryotic transcription, namely how σ factors are autoinhibited. Although it has long been known that $\sigma_{1.1}$ is needed for autoinhibition, quite how it works has been less clear—some studies have pointed to a direct interdomain binding mechanism, others have not. Our data clearly show that in the autoinhibited state, $\sigma_{1.1}$ is juxtaposed with the two DNA binding domains (σ_2 and σ_4) of the σ factor and that this compacted state is held together via complementary electrostatic forces between the domains. For steric reasons, this conformation is incompatible with DNA binding. In performing this work, we have synthesized and successfully applied a new, to the best of our knowledge, trifunctional chemical crosslinking reagent, which will be useful for studying transient interactions in other systems.

EXPERIMENTAL PROCEDURES

NMR Samples

T. maritima σ^A $\sigma_{1.1}$ (residues 1-96 or 1-116, with mutations Q21L, E22V, Q23P, K24R, E25G, T26S, L27H, P28M to install a thrombin site and mutations S96G or S116G to facilitate intein thiolysis and expressed protein ligation) was cloned into the pTXB1 vector (New England Biolabs) to generate a fusion construct of σ^A $\sigma_{1.1}$—*Mxe* GyrA intein—chitin binding domain. BL-21(DE3) (Invitrogen) cells were transformed with this construct, grown overnight on LB plates (100 μg/ml ampicillin) then grown in 1 l M9 minimal media (100 μg/ml ampicillin) with 1.2 g ^{15}NH$_4$SO$_4$ and 2 g ^{13}C glucose as the only nitrogen and carbon sources. The culture was grown at 37°C to an OD$_{600}$ of $\sim$0.6. Expression was induced with 0.8 mM IPTG and was carried out at 30°C for 4.5 h. Bacteria were harvested by centrifugation, resuspended in lysis buffer (500 mM NaCl, 20 mM Tris pH 8.0, 1 mM EDTA) and lysed using a French press. The lysate was centrifuged and the supernatant applied to a chitin bead column (New England Biolabs) and washed extensively with lysis buffer. Intein cleavage was induced with 50 mM DTT in lysis buffer and allowed to proceed overnight at 4°C with gentle rocking. Cleaved protein was eluted with lysis buffer and was exchanged into 1x PBS by dialysis. Thrombin protease (Amersham) was added (50 U) and proteolysis was carried out overnight at room temperature with gentle rocking. The resulting protein was H$_2$N-GSHM-(σ-A 29-95/115)-G-COOH. The sample was further purified by ion exchange chromatography (Hiprep Q16/10 column, AKTA FPLC, Amersham) using a 0.1-1.0 M NaCl gradient in 20 mM Tris·HCl (pH 8.0). Protein samples were characterized by electrospray mass spectrometry (ESMS, Sciex API-100 single quadropole electrospray mass spectrometer). The protein sample was treated at 65°C for 30 min to eliminate *E. coli* proteases and other contaminants and then concentrated in NMR buffer (10 mM NaPi, pH 6.5, 100 mM NaCl, 1 mM EDTA) to a final concentration of 300-800 μM depending on the sample. Protein concentrations were determined using Bradford assay (BioRad) using a BSA (New England Biolabs) standard curve.

NMR Spectroscopy

All NMR experiments were recorded at 25°C using 600, 700, and 800 MHz Bruker Avance NMR spectrometers equipped with cryoprobes. NMR data were processed using Topspin 1.1 (Bruker) and analyzed by NMRView (Johnson, 2004). ^{1}H chemical shifts were referenced to water at 4.75 ppm (at 25°C) and ^{13}C and ^{15}N shifts were derived from indirect referencing. ^{1}H-^{15}N-HSQC,

(C, D) Two-step digestion protocol. Irradiated crosslinker samples of the indicated attachment sites were digested with BNPS-skatole, separated by SDS-PAGE (4–12% acrylamide). Following excision and extraction from the gel, the C-terminal BNPS-skatole fragment (panel C) and N-terminal BNPS-skatole fragment (panel D) were further digested with CNBr and analyzed by SDS-PAGE (10–20% acrylamide, Tris-tricine buffer system) and western blot (HRP-streptavidin).
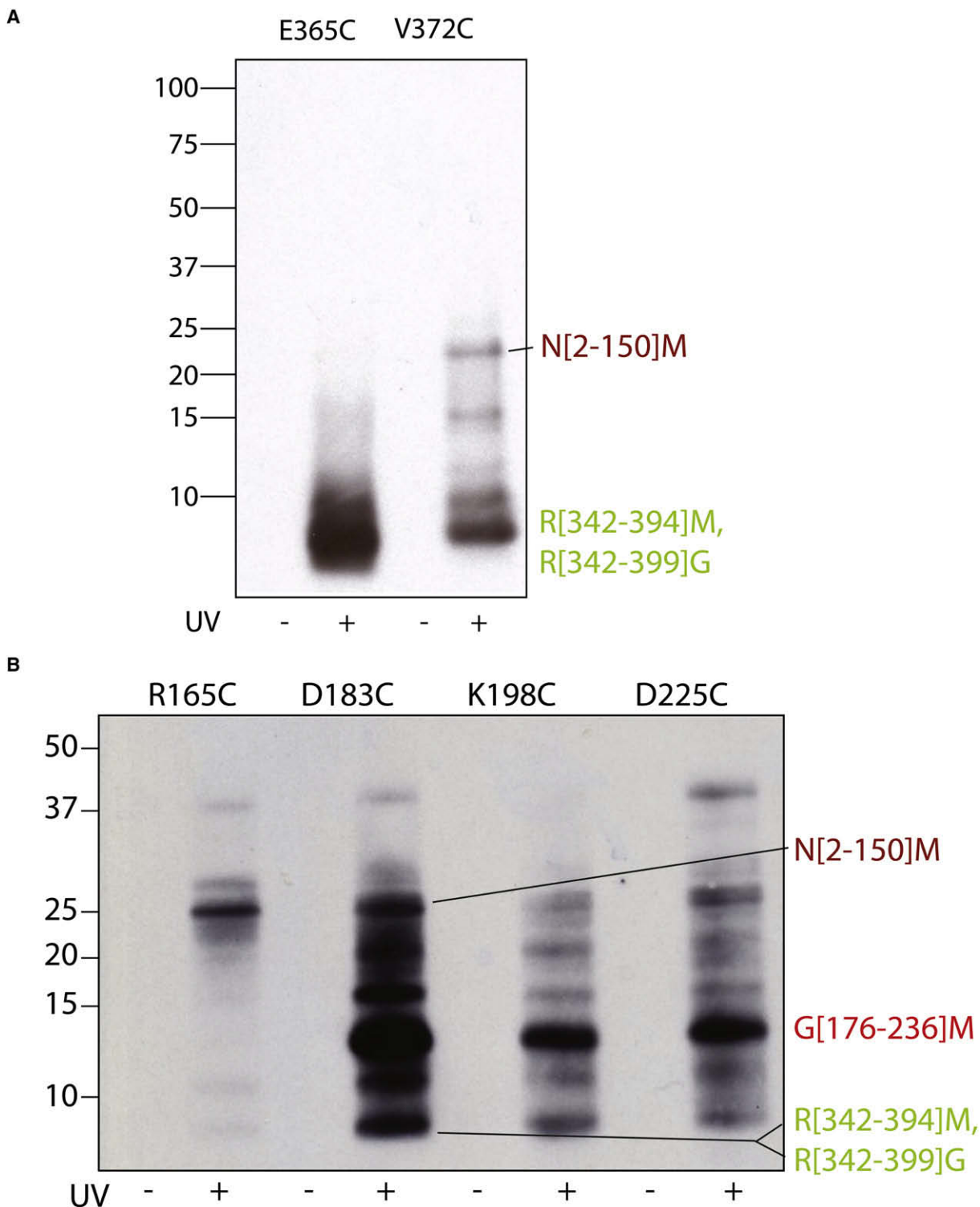
Figure 5. Interdomain crosslinking from σ_4 and σ_2

Crosslinker was attached at the indicated residues within σ_4 (A) and σ_2 (B) through a disulfide. Irradiated (UV+) and nonirradiated (UV-) samples were digested with CNBr, separated by reducing SDS-PAGE (10–20% acrylamide, Tris-tricine buffer system) and probed for biotin by western blotting (HRP-streptavidin). The identity of the labeled bands is shown at right. The N[2-150]M, R[342-394]M, and R[342-399]G bands were identified by mass spectrometry; the G[176-236]M band was identified as described in the text.
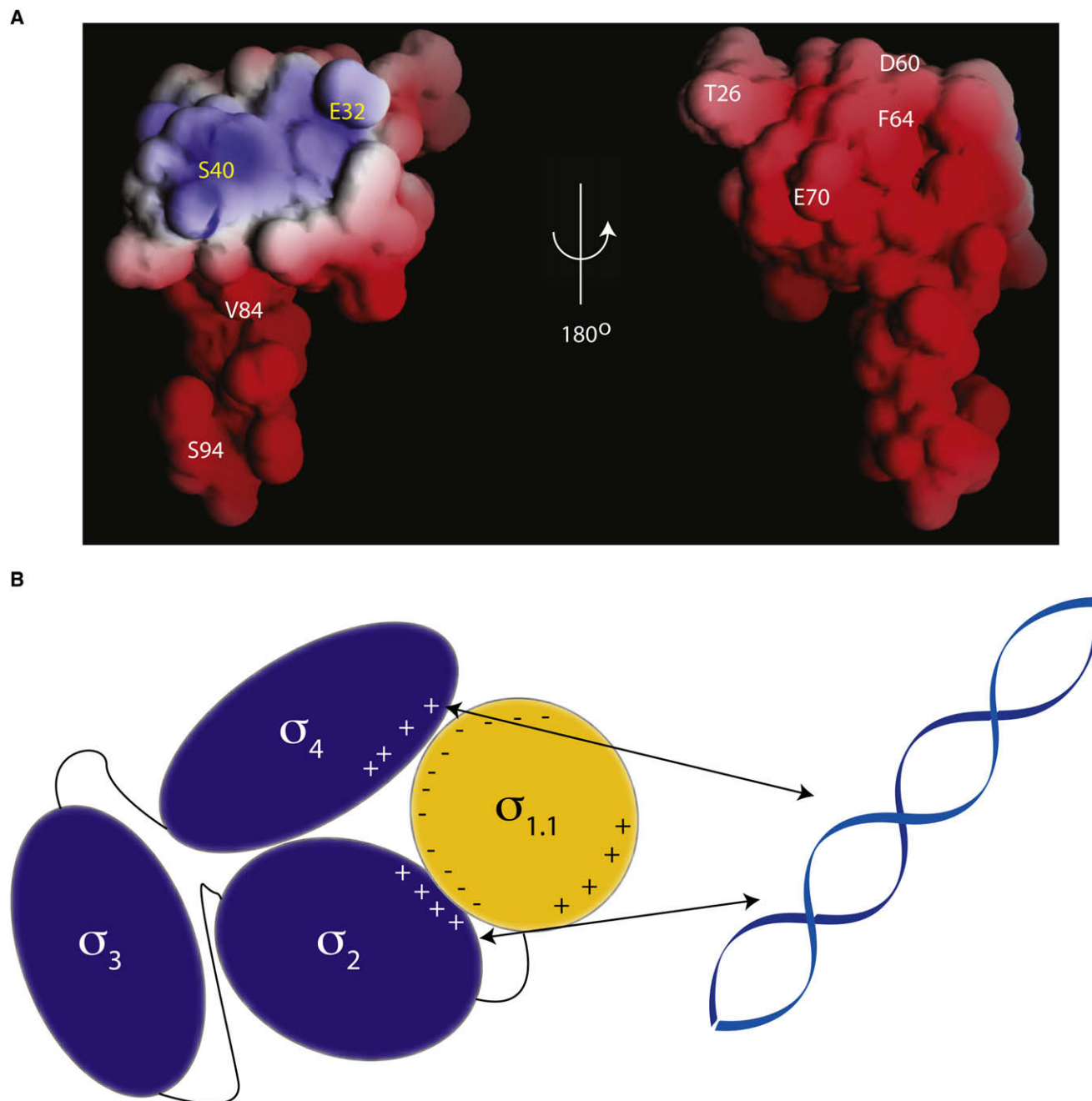
Figure 6. Proposed model of DNA binding inhibition by $\sigma_{1.1}$

(A) Crosslinker attachment sites are indicated on the electrostatic surface map of $\sigma_{1.1}$ generated using the GRASP program. Indicated in white are the sites that were shown to make interdomain crosslinks. Indicated in yellow are the sites from which no interdomain crosslinking was observed.

(B) Schematic showing the compaction model of σ^A autoinhibition. The negative surface of $\sigma_{1.1}$ is capable of forming crosslinks to the DNA binding domains σ_2 and σ_4. It is thus likely that $\sigma_{1.1}$ organizes the σ factor into a compacted structure that is incapable of binding DNA. σ_2 forms crosslinks to σ_4, indicating that these two domains must also be in close proximity.

^{1}H-^{13}C-HSQC, 3D-^{15}N-NOESY-HSQC, HNCO, HNCACB, CBCA(CO)NH experiments were used to obtain the sequential assignment of the backbone (Sattler et al., 1999). Side-chain carbon and proton assignments were obtained using C(CO)NH, HC(CO)NH, HBHA(CO)NH and HCCH-TOCSY experiments. For assigning the aromatic resonances, ^{1}H-^{13}C HSQC, (Hβ)Cβ(CγCδ)Hδ and (Hβ)Cβ(CγCδCϵ)Hϵ (Yamazaki et al., 1993), and 3D ^{13}C NOESY-HSQC data were utilized.

Structure Calculations

Backbone dihedral angles (ϕ and ψ) were calculated by analyzing the ^{13}C$^\alpha$, ^{13}C$^\beta$, ^{13}C′, and ^{15}N chemical shifts with the TALOS program that predicts the backbone torsion angles from the amino acid sequence and chemical shift information (Cornilescu et al., 1999). Hydrogen bond restraints were inferred from slow H/D exchange of backbone amides. Distance restraints were derived from 3D ^{13}C-edited NOESY and 3D ^{15}N-edited NOESY experiments.

Using NMRView, the NOESY cross peak volumes/intensities were obtained and converted into distance restraints using the symmetry ambiguous distance restraints (ADR) protocol within the ARIA program (Linge et al., 2003). A total of 512 structures were calculated using the Cartesian dynamics simulated annealing protocol within ARIA/CNS. The 100 lowest energy structures without any distance and dihedral violations were further refined in water as described by Linge et al. The NMR structures were analyzed using PROCHECK-NMR (Laskowski et al., 1996). The electrostatic potentials were calculated using GRASP (Nicholls et al., 1991). Structures were displayed using MACPymol (Delano Scientific).

Comparison of the calculated structures to existing known protein folds was made using the DALI search engine (Holm and Sander, 1996). The overall fold of three interacting helices is represented in a number of existing structures at high z-score and RMSD in the range 2.5–3.0 Å. However, these structures were of uniformly low sequence similarity (4%–22%) and appeared to have only a topological correspondence of overlapped helices with a similar crossing angle.

Electrophoretic Analysis of Crosslinking Experiments

SDS-PAGE analysis in the crosslinking section was performed using the Criterion system (Biorad). Criterion gels used were 4–12% acrylamide Bis-Tris buffered gels and 10–20% acrylamide Tris-tricine buffered gels, as indicated. Samples for western blotting were separated by SDS-PAGE before being transferred to PVDF (Biorad) using standard western blotting procedures. The membrane was blocked in 5% milk in TBST for 1 h at room temperature then washed three times with TBST and incubated with streptavidin-HRP (GE Health Sciences, 1:5000 in TBST) for 1 h. The membrane was washed three times with TBST and developed using ECL reagents (Perkin Elmer) and Kodak Biomax MR film.

Crosslinking Samples

T. maritima σ^A was cloned into pET15B (Novagen) with an N-terminal hexahistidine tag and a thrombin recognition site for removal of the affinity tag (final sequence: MGSSHHHHHHSSGLVPRGSH-σ^A). Cysteine mutants were generated using the Quikchange II XL kit (Stratagene). All mutations were verified by DNA sequencing. BL-21(DE3) cells were transformed with wild-type or mutant σ^A plasmid and grown in LB broth (100 μg/ml ampicillin) at 37°C to an OD_{600} of ~0.6. Protein expression was induced with 0.8 mM IPTG at 37°C for 4–6 h. Bacteria were harvested by centrifugation, treated at 65°C for 20 min, lysed using a French press, and purified using the Ni-NTA system (Novagen). Protein samples were then transferred to 1x PBS by dialysis and treated with thrombin protease (Amersham, 50 U) overnight at room temperature. Proteolyzed samples were further purified by ion exchange chromatography (HiTrap SP HP, Amersham) with a 0.1–1.0 M NaCl gradient in 20 mM Tris·HCl (pH 8.0). Fractions containing pure protein were concentrated and stored at −80°C in 10% glycerol and at −20°C in 50% glycerol.

Attachment of Crosslinker and Crosslinking

Crosslinker was attached to the purified cysteine mutant of σ^A by disulfide exchange. Details of the crosslinker synthesis can be found in Supplemental Methods. Reaction mixtures contained 6 μM protein and 100 μM crosslinker in 50 mM sodium borate (pH 8.3), 8 mM Tris-HCl (pH 8.3), 80 mM KCl, 0.4 mM EDTA, 5 mM methionine, 0.6 mM tyrosine, 2% glycerol, and 1% DMSO. Reactions were carried out for 20 min at room temperature. Reaction mixtures were then buffer exchanged to 1x PBS using a centrifugal filter device (Vivascience, 10,000 MWCO) and concentrated to approximately 25 μM protein. Crosslinking was then induced by irradiation with a 325 nM HeCd laser for 10–15 s.

CNBr Digestion

CNBr digestion was performed by heating protein (1 mg/ml for crosslinking samples, 5 mg/ml for WT sample used to identify CNBr digestion products) with 1.3% SDS at 42°C for 10 min. Reactions were then carried out in 0.1 N HCl, 100 mM CNBr, 1% SDS overnight at room temperature. Reactions were quenched by neutralization with 1 N NaOH.

BNPS-Skatole Digestion

BNPS-Skatole digestion was performed in 70% acetic acid with ~3.5 mg/ml BNPS-skatole (Sigma) overnight at room temperature. Protein concentration

was 0.5-1 μg/ml depending on the experiment. Following overnight digestion, samples were treated with 67 mM DTT at room temperature for 20 min. Samples were extracted with ether and aqueous fractions were lyophilized and resuspended in SDS loading buffer.

Two-Step Digestion

BNPS-Skatole-digested samples were separated by SDS-PAGE and visualized by Coomassie stain. Bands were excised with a clean razor blade and homogenized in 1 N HCl, ~0.5–1% SDS with mortar and pestle then incubated at 100°C for 5 min. Samples were digested with 100 mM CNBr overnight at room temperature, as described above.

ACCESSION NUMBERS

Atomic coordinates and structure factors are available in the Protein Data Bank (http://www.rcsb.org/) at: 2K6X.

SUPPLEMENTAL DATA

Supplemental data include Supplemental Experimental Procedures and nine figures and can be found with this article online at http://www.chembiol.org/cgi/content/full/15/10/1091/DC1/.

REFERENCES

Barne, K.A., Bown, J.A., Busby, S.J., and Minchin, S.D. (1997). Region 2.5 of the *Escherichia coli* RNA polymerase sigma70 subunit is responsible for the recognition of the 'extended-10' motif at promoters. EMBO J. *16*, 4034–4040.

Borukhov, S., and Nudler, E. (2003). RNA polymerase holoenzyme: structure, function and biological implications. Curr. Opin. Microbiol. *6*, 93–100.

Bowers, C.W., and Dombroski, A.J. (1999). A mutation in region 1.1 of σ^{70} affects promoter DNA binding by *Escherichia coli* RNA polymerase holoenzyme. EMBO J. *18*, 709–716.

Browning, D.F., and Busby, S.J. (2004). The regulation of bacterial transcription initiation. Nat. Rev. Microbiol. *2*, 57–65.

Burgess, R.R., Travers, A.A., Dunn, J.J., and Bautz, E.K. (1969). Factor stimulating transcription by RNA polymerase. Nature *221*, 43–46.

Callaci, S., Heyduk, E., and Heyduk, T. (1999). Core RNA polymerase from *E. coli* induces a major change in the domain arrangement of the sigma 70 subunit. Mol. Cell *3*, 229–238.

Camarero, J.A., Shekhtman, A., Campbell, E.A., Chlenov, M., Gruber, T.M., Bryant, D.A., Darst, S.A., Cowburn, D., and Muir, T.W. (2002). Autoregulation of a bacterial σ factor explored by using segmental isotopic labeling and NMR. Proc. Natl. Acad. Sci. USA *99*, 8536–8541.

Campbell, E.A., and Darst, S.A. (2005). Regulation of bacterial transcription by anti-s factors. In Structural Biology of Bacterial Pathogenesis, G. Waksman, M. Caparon, and S. Hultgren, eds. (Washington, DC: ASM Press), pp. 1–15.

Campbell, E.A., Masuda, S., Sun, J.L., Muzzin, O., Olson, C.A., Wang, S., and Darst, S.A. (2002a). Crystal structure of the *Bacillus stearothermophilus* anti-sigma factor SpoIIAB with the sporulation sigma factor sigmaF. Cell *108*, 795–807.

Campbell, E.A., Muzzin, O., Chlenov, M., Sun, J.L., Olson, C.A., Weinman, O., Trester-Zedlitz, M.L., and Darst, S.A. (2002b). Structure of the bacterial RNA polymerase promoter specificity sigma subunit. Mol. Cell 9, 527–539.

Campbell, E.A., Tupy, J.L., Gruber, T.M., Wang, S., Sharp, M.M., Gross, C.A., and Darst, S.A. (2003). Crystal structure of Escherichia coli σ^E with the cytoplasmic domain of its anti-σ RseA. Mol. Cell 11, 1067–1078.

Campbell, E.A., Westblade, L.F., and Darst, S.A. (2008). Regulation of bacterial RNA polymerase sigma factor activity: a structural perspective. Curr. Opin. Microbiol. 11, 121–127.

Cavanagh, J., Fairbrother, J.W., Palmer, A.G., III, and Skelton, N.J. (1996). Protein NMR Spectroscopy; Principles and Practice, First Edition (San Diego, CA: Academic Press).

Cornilescu, G., Delaglio, F., and Bax, A. (1999). Protein backbone angle restraints from searching a database for chemical shift and sequence homology. J. Biomol. NMR 13, 289–302.

Darst, S.A. (2001). Bacterial RNA polymerase. Curr. Opin. Struct. Biol. 11, 155–162.

Dombroski, A.J., Walter, W.A., Record, M.T.J., Siegele, D.A., and Gross, C.A. (1992). Polypeptides containing highly conserved regions of transcription initiation factor sigma-70 exhibit specificity of binding to promoter DNA. Cell 70, 501–512.

Dombroski, A.J., Walter, W.A., and Gross, C.A. (1993). Amino-terminal amino acids modulate sigma-factor DNA-binding activity. Genes Dev. 7, 2446–2455.

Ebright, R.H. (2000). RNA polymerase: structural similarities between bacterial RNA polymerase and eukaryotic RNA polymerase II. J. Mol. Biol. 304, 687–698.

Gardella, T., Moyle, H., and Susskind, M.M. (1989). A mutant Escherichia coli sigma 70 subunit of RNA polymerase with altered promoter specificity. J. Mol. Biol. 206, 579–590.

Gross, C.A., Chan, C., Dombroski, A., Gruber, T., Sharp, M., Tupy, J., and Young, B. (1998). The functional and regulatory roles of sigma factors in transcription. Cold Spring Harb. Symp. Quant. Biol. 63, 141–155.

Gruber, T.M., and Gross, C.A. (2003). Multiple sigma subunits and the partitioning of bacterial transcription space. Annu. Rev. Microbiol. 57, 441–466.

Hinton, D.M., Vuthoori, S., and Mulamba, R. (2006). The bacteriophage T4 inhibitor and coactivator AsiA inhibits Escherichia coli RNA polymerase more rapidly in the absence of sigma70 region 1.1: evidence that region 1.1 stabilizes the interaction between sigma70 and core. J. Bacteriol. 188, 1279–1285.

Holm, L., and Sander, C. (1996). Mapping the protein universe. Science 273, 595–603.

Johnson, B.A. (2004). Using NMRView to visualize and analyze the NMR spectra of macromolecules. Methods Mol. Biol. 278, 313–352.

Kobe, B., and Kemp, B.E. (1999). Active site-directed protein regulation. Nature 402, 373–376.

Lane, W.J., and Darst, S.A. (2006). The structural basis for promoter −35 element recognition by the group IV sigma factors. PLoS Biol. 4, e269. Published online August 15, 2006. 10.1371/journal.pbio.0040269.

Laskowski, R.A., Rullmannn, J.A., MacArthur, M.W., Kaptein, R., and Thornton, J.M. (1996). AQUA and PROCHECK-NMR: programs for checking the quality of protein structures solved by NMR. J. Biomol. NMR 8, 477–486.

Linge, J.P., Habeck, M., Rieping, W., and Nilges, M. (2003). ARIA: automated NOE assignment and NMR structure calculation. Bioinformatics 19, 315–316.

Malhotra, A., Severinova, E., and Darst, S.A. (1996). Crystal structure of a sigma 70 subunit fragment from E. coli RNA polymerase. Cell 87, 127–136.

Mekler, V., Kortkhonjia, E., Mukhopadhyay, J., Knight, J., Revyakin, A., Kapanidis, A.N., Niu, W., Ebright, Y.W., Levy, R., and Ebright, R.H. (2002). Structural organization of bacterial RNA polymerase holoenzyme and the RNA polymerase-promoter open complex. Cell 108, 599–614.

Murakami, K.S., and Darst, S.A. (2003). Bacterial RNA polymerases: the wholo story. Curr. Opin. Struct. Biol. 13, 31–39.

Murakami, K.S., Masuda, S., Campbell, E.A., Muzzin, O., and Darst, S.A. (2002a). Structural Basis of Transcription Initiation: An RNA Polymerase Holoenzyme-DNA Complex. Science 296, 1285–1290.

Murakami, K.S., Masuda, S., and Darst, S.A. (2002b). Structural basis of transcription initiation: RNA polymerase holoenzyme at 4 A resolution. Science 296, 1280–1284.

Muralidharan, V., and Muir, T.W. (2006). Protein ligation: an enabling technology for the biophysical analysis of proteins. Nat. Methods 3, 429–438.

Nicholls, A., Sharp, K.A., and Honig, B. (1991). Protein folding and association: insights from the interfacial and thermodynamic properties of hydrocarbons. Proteins 11, 281–296.

Ottesen, J.J., Blashke, U.K., Cowburn, D., and Muir, T.W. (2003). In Biological Magnetic Resonance, N.R. Krishna and L.J. Berliner, eds. (New York: Kluwer Academic), pp. 35–51.

Sattler, M., Schleucher, J., and Griesinger, C. (1999). Heteronuclear multidimensional NMR experiments for the structure determination of proteins in solution employing pulse field gradients. Prog. Nucl. Magn. Reson. Spectrosc. 34, 93–158.

Siegele, D.A., Hu, J.C., Walter, W.A., and Gross, C.A. (1989). Altered promoter recognition by mutant forms of the sigma 70 subunit of Escherichia coli RNA polymerase. J. Mol. Biol. 206, 591–603.

Sorenson, M.K., and Darst, S.A. (2006). Disulfide cross-linking indicates that FlgM-bound and free σ28 adopt similar conformations. Proc. Natl. Acad. Sci. USA 103, 16722–16727.

Sorenson, M.K., Ray, S.S., and Darst, S.A. (2004). Crystal structure of the flagellar sigma/anti-sigma complex sigma-28/FlgM reveals an intact sigma factor in an inactive conformation. Mol. Cell 14, 127–138.

Travers, A.A., and Burgess, R.R. (1969). Cyclic re-use of the RNA polymerase sigma factor. Nature 222, 537–540.

Vassylyev, D.G., Sekine, S.-i., Laptenko, O., Lee, J., Vassylyeva, M.N., Borukhov, S., and Yokoyama, S. (2002). Crystal structure of a bacterial RNA polymerase holoenzyme at 2.6 A resolution. Nature 417, 712–719.

Vuthoori, S., Bowers, C.W., McCracken, A., Dombroski, A.J., and Hinton, D.M. (2001). Domain 1.1 of the sigma-70 subunit of Escherichia coli RNA polymerase modulates the formation of stable polymerase/promoter complexes. J. Mol. Biol. 309, 561–572.

Wilson, C., and Dombroski, A.J. (1997). Region 1 of σ^70 is required for efficient isomerization and initiation of transcription by Escherichia coli RNA polymerase. J. Mol. Biol. 267, 60–74.

Wishart, D.S., and Sykes, B.D. (1994). The 13C chemical-shift index: a simple method for the identification of protein secondary structure using 13C chemical-shift data. J. Biomol. NMR 4, 171–180.

Yamazaki, T., Forman-Kay, J.D., and Kay, L.E. (1993). Two-dimensional NMR experiments for correlating C-13b and H-1d/e chemical shifts of aromatic residues in 13C-labeled proteins via scalar couplings. J. Am. Chem. Soc. 115, 11054–11055.